

# We are IntechOpen, the world's leading publisher of Open Access books Built by scientists, for scientists

5,600

Open access books available

137,000

International authors and editors

170M

Downloads

Our authors are among the

154

Countries delivered to

TOP 1%

most cited scientists

12.2%

Contributors from top 500 universities



WEB OF SCIENCE™

Selection of our books indexed in the Book Citation Index  
in Web of Science™ Core Collection (BKCI)

Interested in publishing with us?  
Contact [book.department@intechopen.com](mailto:book.department@intechopen.com)

Numbers displayed above are based on latest data collected.  
For more information visit [www.intechopen.com](http://www.intechopen.com)



# Wave-Forced Dynamics at Microtidal River Mouths

*Maurizio Brocchini, Matteo Postacchini, Lorenzo Melito, Eleonora Perugini, Andrew J. Manning, Joseph P. Smith and Joseph Calantoni*

## Abstract

Microtidal river mouths are dynamic environments that evolve as a consequence of many forcing actions. Under the hydrodynamic viewpoint, river currents, sea waves and tides strongly interact, and their interplay determines specific sediment transport and morphological patterns. Beyond literature evidence, information comes from field observations made at the Misa River study site, a microtidal river along the Adriatic Sea (Italy), object of a long-going monitoring. The river runs for 48 km in a watershed of 383 km<sup>2</sup>, providing a discharge of about 400 m<sup>3</sup>/s for return periods of 100 years. The overall hydrodynamics, sediment transport and morphological evolution at the estuary are analyzed with particular attention to specific issues like: the generation of vortical flows at the river mouth, the influence of various wave modes (infragravity to tidal) propagating upriver, the role of sediment flocculation, the generation and evolution of bed features (river-mouth bars and longitudinal nearshore bars). Numerical simulations are also used to clarify specific mechanisms of interest.

**Keywords:** estuarine dynamics, river-sea interaction, river current, tide, infragravity waves, sandbars, microtidal

## 1. Introduction

Estuaries are dynamic and complex environments. Estuarine hydrodynamics are the product of nonlinear interactions between freshwater flow, tidal, wave, and wind forcing, and bathymetric and topographic changes [1, 2]. Such processes directly affect sediment transport and the morphodynamics of the estuary, which may lead to the formation of complex morphological patterns like river mouth bars [3] and submerged sandbars [4].

Although the influence of classical riverine and marine hydrodynamic forcing mechanisms, such as gravity waves and tides, are typically accounted for to describe the estuarine dynamics, an increasing number of studies is focusing on infragravity (IG hereafter) waves, which are seen to play a non-negligible role in estuary evolution [5]. IG waves are a specific type of low-frequency waves with periods between 20 and 30 seconds to 5 minutes, larger than those of sea/swell waves [6, 7]. Typically, IG waves are generated either (i) as long waves bound to short wave groups,

or (ii) by a temporal variation of the breakpoint, or (iii) from swell–swell interactions [8–10].

IG waves are regarded as an important trigger of sandbar generation in the coastal area, especially in the short term, although their role has not been properly understood so far [11, 12]. IG waves are also thought to be of some importance for sediment transport and nearshore morphodynamics, though not a primary forcing [13]. For instance, during storms, breakers mobilize a large quantity of sediment, whose transport is modulated by IG waves [14].

In general, subtidal bars generating and evolving along sandy coasts are typical of wave-dominated environments as a whole and are the result of complex hydrodynamic and sediment transport patterns taking place within the surf zone [11, 15]. Sandbars exist both close to and far from river mouths, due to their strong link to the marine forcing, although their behavior is largely affected by river current and sediment transport, as well as by artificial structures existing at the mouth [4, 16, 17]. Since sandbars promote wave breaking and energy dissipation, they represent a natural solution for beach protection and are fundamental for coastal stability in both short term (storm scale) and long term (scale of years/decades) timescales [18, 19]. Several studies focused on the definition of evolutionary patterns for sand bars. It is commonly acknowledged that waves break over the bars during sea storms and generate undertow profiles, which lead to sediment being advected seaward and sandbars migrating offshore. Conversely, although with some notable exceptions [20], onshore bar motion is typically observed under non-breaking waves and relatively mild wave climate, like that occurring in summertime [12, 21–23].

Evidence shows that IG waves can easily enter a river mouth and propagate upriver for long distances, even during fast river flow conditions. The presence of IG waves in the estuarine regions has been put in relation to edge waves entering the estuary and producing resonance, while IG wave modulation by tides has been observed along the Pescadero River (North California), Ría de Santiuste (Spain), the Albufeira Lagoon (Portugal) and the Misa River (Italy) [1, 24–26].

River mouth bars are morphological features that generate and evolve due to the direct effect of riverine currents and marine actions (waves, tides). Typically, the sediment transported via river flow deposits out of the mouth, at a distance of about twice the river width, due to flow expansion [27–29]. Nevertheless, the location where the bar is formed depends on the amount of sediment transport induced by the river discharge and the net residuals of marine actions. Therefore, in a wave-dominated environment, sediment deposits can also be present inside the river mouth and lead to mouth bars. Such bars are extremely relevant for the overall estuarine dynamics, potentially obstructing the river cross-section to the point of contributing to flooding or river overflows. Downriver migration of the bar occurs when the river discharge dominates the estuarine dynamics and the increased flow velocity on the bar crest is able to erode the sediment on the top, which then deposits seaward because of flow deceleration [30]. On the other hand, weak river flows associated with comparatively more intense sea actions induce sediment accumulation and upriver migration of the bar.

Due to higher concentration values with respect to both upriver and river-mouth regions, a “sediment trap” can be generated in the upper estuary due to both suspended matter and residual circulation. A clay content of >5–10% can make fine-grained sediments behave in a cohesive manner [31, 32]. The sediment grains, and often “sticky” natural organic matter that is present, cause sediment particles to cease acting independently. The behavior is typically characterized by flocculation (i.e., individual sediment particles interact and “bond”), a process whereby cohesive and fine-grained mixed sediment particles have the potential to aggregate into

flocs [33, 34], which contribute to the formation of near-bed suspension layers in estuaries and may alter water column turbulent mixing, rheology, and sedimentary particle residence (retention) times.

Experiments have shown that when the fine fraction and the larger non-cohesive sediments coexist as a single mixture in an estuary [31], there exists the potential for the two fractions to combine and exhibit some degree of interactive flocculation [35, 36]. Further, cohesive sediments that are mixed into a predominantly cohesionless sandy region can create a 'cage-like' structure that can fully encompass the sand grains, thereby trapping the sand within a clay floc envelope [37]. The degree of cohesion between the various sediment fractions tends to increase with the content of fine clay minerals within the sediment, especially for clay contents larger than 5–10% [37–40], with the biological activity playing an important role in the flocculation of mixed suspensions [41]. In terms of properties, the floc size ranges from microns to centimeters and their effective density generally decreases with size [42–44], while their settling velocity follows a size-dependent Stokes law settling relationship [45, 46]. Due to their fast settling velocities [47, 48], macroflocs tend to have the most influence on the mass settling flux [49].

To investigate the interplay between the characteristic processes of microtidal estuarine environments and their effects in the nearby river reach and coastal area, field observations have been performed along the Misa River (MR hereafter) and its estuary, with dedicated field campaigns [50, 51] and long-term measurements collected using both on-site instrumentation and remote sensors [4, 26, 52]. The present work illustrates a comprehensive overview of recent observations and analyses performed to achieve a better understanding of estuarine dynamics at a microtidal river mouth, from the hydrological, morphodynamic, and sedimentological viewpoints.

The chapter is divided as follows. Section 2 describes the field campaigns and the instrumentation deployed along the MR and at the estuary, while the main results are reported in Section 3. An overall discussion, followed by some concluding remarks, is presented in Section 4.

## **2. Materials and methods**

Both short-term and long-term monitoring was carried out at the MR estuary. Specifically, two field campaigns were carried out in September 2013 and January 2014 in the most downstream part of the MR and within the nearby coastal area [50, 51]. Additionally, long-term measurements are being collected since 2015, with a set of instrumentation installed in river and sea, as well as using remote sensors. Numerical simulations are also used to support both experimental findings and speculations, and to better understand the complex dynamics at the MR estuary.

### **2.1 Study site**

The MR runs from the Apennine Mountains (central Italy) to Senigallia (Marche Region), where it flows into the Middle Adriatic Sea after about 48 km. The MR is characterized by a 383 km<sup>2</sup> watershed and its flow rate is around 400, 450, and 600 m<sup>3</sup>/s for return periods of 100, 200, and 500 years, respectively. While a low-flow regime is promoted by a relatively small amount of precipitation in the MR watershed during the summer, significantly higher flow regime characterizes the wintertime [50, 51].



An illustration of the coastal and offshore area is provided in **Figure 1a**, with a close-up view of the nearshore and estuarine regions shown in **Figure 1b**. The most downstream portion of the MR is also shown in **Figure 1c**. The final reach features a heavily engineered river mouth, characterized by cement walls in place of classical riverbanks, which allows one to easily collect and analyze the hydro-morphodynamic data of the microtidal environment. The beach located north of the estuary and harbor is protected by emerged rubble-mound breakwaters, while the southern natural beach is protected by multiple alignments of longshore sandbars (**Figure 1b**).

From a hydrological viewpoint, the MR estuary is classified as a salt-wedge estuary, where the water column is split into two parts: the outgoing river current flows in the upper portion, while the entering seawater flows in the lower portion [53]. The salt-wedge behavior, i.e. the simultaneous existence of saltwater and freshwater within the water column extends some kilometers seaward, as confirmed by salinity measurements collected up to 2 km from the estuary [50].



**Figure 1.** Instrumentation employed for the MR monitoring: a) locations of the ADCP and tide gauge in the coastal region; b) locations of sensors displaced within the final reach of the river and the offshore area; c) locations of the two river gauges. Photos illustrating: d) the river portion near the RG1 instrument; e) the ADCP deployed at the MEDA station.

Soil samples were collected within the lower MR reach and confirmed the presence of clay, characterized by high percentages of montmorillonite minerals. Such fine-grained clay sediments promote formation of flocs, i.e. aggregations of individual clay and other fine particles, organic matter, micro-algae and bacteria, and other reactive constituents. Based on both salinity measurements and the sampled clayey material at the riverbed, it was speculated the existence of an upriver flocculation zone (between 2 km and 700 m from the mouth), with salinity  $S < 10$  psu, and a downstream deposition zone (between 700 m from the mouth and the mouth itself), with  $S > 10$  psu [50, 51].

The MR is characterized by large sediment transport rates despite the moderate flow rate, similar to many rivers originating within the Apennine Mountains. Such intense sediment outflow supplies a large amount of material to the coastal areas around the estuary, this being true especially for the natural beach located south of the estuary, which presents an array of longshore sandbars with a long-term morphological evolution [4, 16].

## 2.2 Short-term and long-term measurements

Within the framework of two international projects funded by the Office of Naval Research Global (UK), named EsCoSed (“ESTuarine COhesive SEDiments”) and MORSE (“Modeling and Observation of River-Sea Exchanges at a microtidal estuary”), a series of activities have been planned in the last decade within the microtidal estuary of the MR.

### 2.2.1 The EsCoSed project

During the EsCoSed project, two field campaigns were carried out in September 2013 and January 2014 with the purpose of investigating, respectively, the summertime regime, mainly characterized by low-flow conditions, and the wintertime regime, where low-flow conditions alternate to high-flow conditions [50, 51]. Observations of meteorology, hydrodynamics and morphodynamics were performed using instrumentation deployed for some days during both investigated periods. Furthermore, in the wintertime experiment, water and sediment were sampled within the river and estuary, as well as in the sediment plume generated during high-flow/stormy conditions.

The hydro-morphodynamic parameters were recorded using small quadpods (an overall height of  $\sim 1$  m and a roughly square base of  $\sim 1$  m<sup>2</sup>) both in the final MR reach and in the nearby sea, up to 7-m depth. The quadpods were specifically devised to accommodate a set of instruments for the measurement of water velocity profiles along the water column (six velocity profilers), seabed variations (two pencil beams), the turbidity along the lower portion of the water column (two CT probes), and wave characteristics (one Sentinel 1200KHz Acoustic Doppler Current Profiler - ADCP, from Teledyne RDI®, deployed at a depth of  $\sim 7$  m). The quadpod locations in the 2013–2014 experiments are shown in **Figure 1b** as red and blue triangles, respectively indicating quadpods deployed in the river (QR1, QR2, QR3) and sea (QS1, QS2, QS3). Additionally, information on both water surface level at further locations and surface current were collected using, respectively, two tide gauges (TGup, TGdown) and Lagrangian drifters launched into the final reach of the MR.

Finally, a video-monitoring station named “Sena Gallica Speculator” (SGS) was installed at the Senigallia harbor in 2015 and is currently operating. The station is composed of four cameras located on top of a tower and is oriented to encompass



the mouth of the MR and a coastal area located between the MR estuary and a pier, called “Rotonda a Mare” and located 500 m south of the estuary [4].

### 2.2.2 The MORSE project

The MORSE project aimed at providing a long-term monitoring of the MR estuary and adjacent portions of river and sea, through the deployment of onsite instrumentation in 2018 [52, 54].

First, a Workhorse Sentinel 300 kHz ADCP (Teledyne RDI®) for the measurements of offshore wave conditions (**Figure 1e**) was installed within the MEDA station, a meteo-marine station located  $\sim 1.5$  nm north of Senigallia and 1.5 nm from the coast (purple triangle in **Figure 1a**). The station is property of the Italian National Research Council (CNR) and is additionally equipped with several sensors for the monitoring of both atmosphere and sea water.

A tide gauge was deployed within a protected area at the entrance of the Senigallia harbor to record tidal excursions and storm surges (green triangle in **Figure 1a**).

Finally, a stream gauge was installed within the MR for flow-rate measurements, which is fundamental for the understanding of river-sea interactions. The chosen site is located about 1.2 km upriver of the mouth, near the bridge known as “Ponte Garibaldi”, and very close to a pre-existent hydrometer, property of the Civil Protection (Marche Region), installed for the measurement of the river stages. Both the hydrometer and the stream gauge, the location of which is collectively indicated here as RG1 (**Figure 1c**), are employed to observe upriver wave propagation from the MR mouth. The RG1 hydrometer complements another hydrometer located at “Bettolelle” (here referred as RG2), about 10 km from the estuary (**Figure 1c**).

The data collected by some of the above-mentioned instruments are represented in **Figure 2**. These can be profitably used as initial or boundary conditions for the initialization and validation of the numerical modeling of the MR estuary, as illustrated in the following.

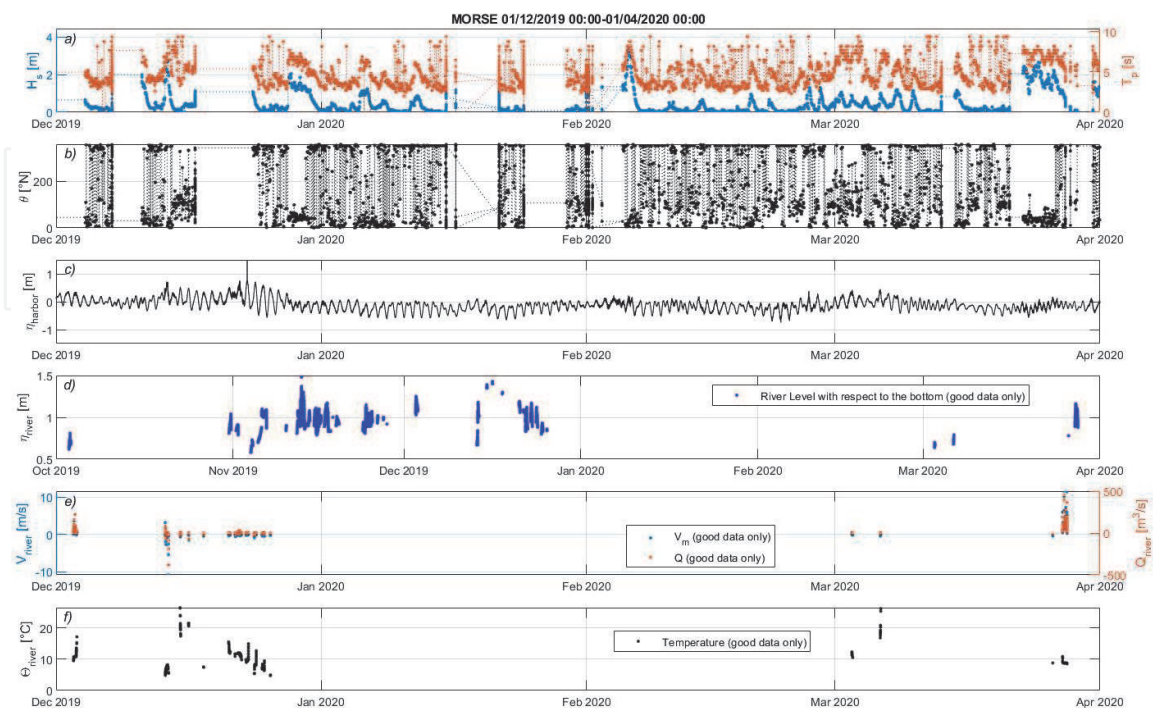


**Figure 2.**

Overall view of the data collected from December 2019 to April 2020. (a) Significant wave height and (b) peak period measured by the offshore ADCP at the MEDA station. (c) Water-surface level at Senigallia harbor. (d) Water-surface level, (e) mean speed and discharge, (f) temperature at the RG1 stream gauge.

## 2.3 Numerical modeling

The large amount of observed data allowed us to set up a numerical model of the MR estuarine area using the Delft3D software suite [55, 56]. A two-dimensional, depth-averaged model was used to reproduce the hydro-morphodynamics occurring along the final stretch of the MR estuarine channel [54]. Specifically, a coupled WAVE-FLOW simulation was performed to investigate the deformation and displacement of the river mouth bar under the actions of river current and waves. The WAVE model was forced using time series of wave height, period and direction recorded at the offshore MEDA station. The time series of the water level recorded at the tide gauge was instead used for a first validation of the model.

## 3. Results

Observations and results coming from both short-term and long-term recordings are reported in the following. The local dynamics observed during the 2013–2014 experiments are first described, with focus on the main seasonal differences in the hydrodynamics and the interplay between river and marine forcing actions in winter, as well as the saltwater-freshwater interaction across the water column (Section 3.1). Insight from a flocculation model supports the observed local dynamics (Section 3.2). The wave entrance in the MR estuary and the upriver propagation of long-wave modes are detailed in Section 3.3. The morphological processes occurring within the lower river reach (Section 3.4) and in the nearshore area south of the MR estuary (Section 3.5) are finally described, with special focus on the bar evolution.

### 3.1 Local dynamics

The estuarine area of the MR is subjected to sea storms mainly coming from two directions, as typically observed in coastal regions of the Middle Adriatic Sea. Short, steeper waves generated by WNW, N or NNE (Bora) winds typically enter the MR mouth, since their incoming direction is almost perfectly aligned to the estuary orientation. Also relevant in the MR environment are the ESE-approaching waves, induced by Sirocco winds. Such waves are significantly angled and cannot easily enter the MR. Consequently, Sirocco waves are reflected by the river walls and strongly affect the morphology around the estuary, thus impacting on the evolution of nearby sandbars [4].

Significant differences exist between summertime and wintertime conditions in terms of wind and rainfall, these directly affecting the wave action and the river current interplaying at the MR estuary. Specifically, the wind blowing during the investigated periods promoted the generation of waves of different heights, which mainly depended on the wind direction rather than on its velocity. The wind direction was frequently changing during the summertime experiment, whereas two intense storms were observed in wintertime and were characterized by almost constant wind directions.

During mild/quiescent conditions in both summer and winter (i.e. time intervals before and after storms), an upriver flow propagation was observed very close to the MR estuary (at QR3, i.e. 290 m upriver), with farther inland locations (QR2, i.e. around 400 m upriver) presenting a significant tidal modulation of the water column. An enhanced salt-wedge behavior was also observed during the wintertime experiment [57]. However, some differences arise between quiescent conditions occurring in summer and winter. Specifically, the marine action in summertime was



comparable to the river forcing, as confirmed by the observed tracks of surface drifters deployed within the final reach of the MR. Recorded surface speeds in summer are generally smaller than those recorded in winter, with the surface flow being slowed down and sometimes reversed due to upriver-propagating waves and tide. Conversely, drifter deployed before and after the two winter storms showed an increasing surface velocity while moving downstream. Such behavior is further supported by recorded velocity profiles across the water column at QR2 and QR3 locations, which followed a marked salt-wedge pattern, additionally modulated by the tidal motion [51].

Hydraulic data recorded during the January 2014 experiment are illustrated in **Figure 3**. The stage at RG2 and the mean precipitation within the MR watershed are shown in **Figure 3a**. The two floods are here highlighted by the stage peaks occurred in the mornings of 25 and 28 January, almost simultaneous to high-tide conditions recorded at Ancona harbor (**Figure 3b**) and to the sea storms recorded at QS3 (significant height and peak periods are illustrated in **Figure 3c**). The instantaneous velocity magnitude recorded along the water column at QR2 are plotted in **Figure 3d**.

The increased river outflow during the January 2014 storms generated a large river plume with a considerable amount of sediment extending up to around 1.3 km offshore of the mouth. The occurrence of strong river outflow was coupled with a negligible modulation provided by tidal oscillation on the velocity distribution along the water column, especially at a relatively far distance from the mouth (e.g., at QR2). Additionally, during the winter storms a large sediment deposition was observed closer to the mouth (i.e., near the bend, at QR3), due to the convergence of hydrodynamic fluxes and suspended sediments from both river and sea. This also suggests the existence of a turbidity maximum zone (TMZ), typically observed in macro- and meso-tidal estuaries, but rarely in microtidal environments [58–60]. Although TMZs were observed during both winter storms, their vertical structure was different and depended on the energetic nature of the storms. The storm occurred during 28–29 January 2014 was much less intense than that occurred

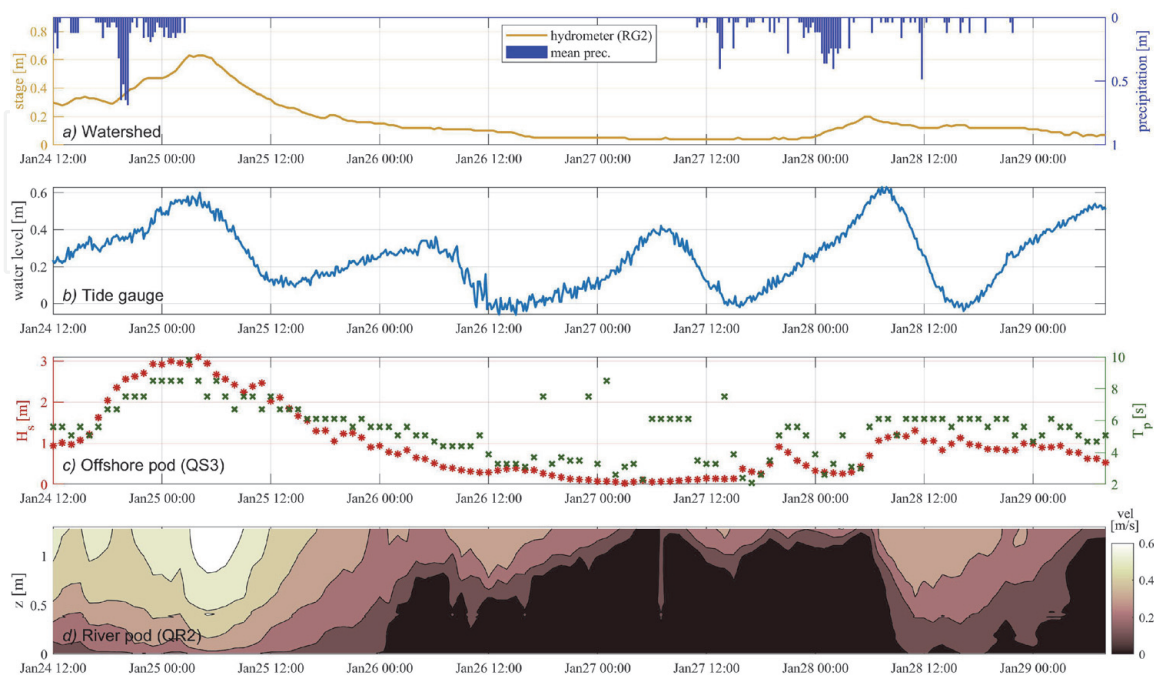


**Figure 3.** Observed environmental conditions during the January 2014 experiment: (a) precipitation in the watershed and stage at RG2, (b) water surface level recorded by tide gauge (Ancona), (c) offshore wave characteristics recorded at QS3, (d) velocity distribution along the water column.

during 24–25 January 2014, especially in terms of incoming wave height and outgoing river flow. A relatively larger turbidity was observed during the smaller storm [57].

While the summer period is supposed to be characterized by a flocculation region at distances larger than 600 m upstream of the MR mouth and by large sediment deposition throughout the final river reach, wintertime stormy conditions enhanced the sediment transport and provided different morphological patterns due to the strong interplay between incoming and outgoing fluxes: 1) a relevant erosion upstream of QR3, where the river discharge dominates on the marine forcing; 2) an erosion/deposition pattern downstream of QR3 and at the mouth; 3) a modification of the rheological properties of the soil both at the MR mouth and within the river-plume area [50, 51].

### 3.2 Floc dynamics

To investigate the potential depositional effects within the Misa system, a rigorously proven flocculation model (FM) suite was used [47, 48, 61, 62]. The FM is built on a series of empirical-derived algorithms that can quantitatively assess the relative settling and mass flux dynamics for both pure mud flocs and floc populations derived from a range of mud-sand mixtures. It is based on flocculation concept of macroflocs ( $D > 160 \mu\text{m}$ ) and microflocs ( $D < 160 \mu\text{m}$ ), as outlined in the classic 'order of aggregation' [63, 64]. FM outputs include macrofloc/microfloc settling velocity, ratio of floc mass between the two size fractions and the total mass settling flux (MSF).

The MR estuary has been subdivided into three regions with different representative sediment compositions, two located 600 m and 100 m upriver of the estuary, one located 400 m off the estuary. A nominal representative mud:sand (M:S) composition of 100 M:0S is chosen at the inland site, 50 M:50S equal mud/sand mixture at the mid-zone, and pure sand (0M:100S) in the seaward region, based on the collected field data [50, 51]. The level of flocculation primarily depends upon the combined effects of Suspended Sediment Concentration (SSC) and turbulent mixing. Hence, the FM indicated a fast macrofloc settling (3.5 mm/s at shear stress of 0.35 Pa) and a relatively quick microfloc settling at the pure cohesive inland generated during small storm conditions (28–29 January 2014). Further, both the lower river and seaward zones were much less turbid. In the lower river, the less cohesive equally mixed sediment composition produced slower macroflocs and quicker microflocs than within the inland region, with an equal apportioning of floc mass between macro- and microfloc fractions. The seaward (pure-inert/non-flocculating) sediment settled fast at  $\sim 6.8$  mm/s.

Throughout the Misa system, the MSF was only  $\sim 40\%$  of that occurring during small storm conditions. Quiescent conditions (27 January 2014) saw a further 20–25% slowing in the floc settling velocities, with SSC being only 30–40% of that found during the small storm at each site. Specifically, the FM indicated that quiescent conditions favored smaller microfloc fraction dynamics, a much tighter spatial grouping and significantly smaller settling flux values.

### 3.3 Upriver propagation of long waves

IG waves are long-wave modes that are seen to easily propagate upriver in meso- and macro-tidal estuaries [1, 24, 25], while their impact on microtidal estuaries has been rarely investigated. Upriver propagation of IG waves were observed in the microtidal environment of the MR during the January 2014 experiment (**Figure 4a–c**) [26]. The dominant generation mechanism of IG waves in this case is

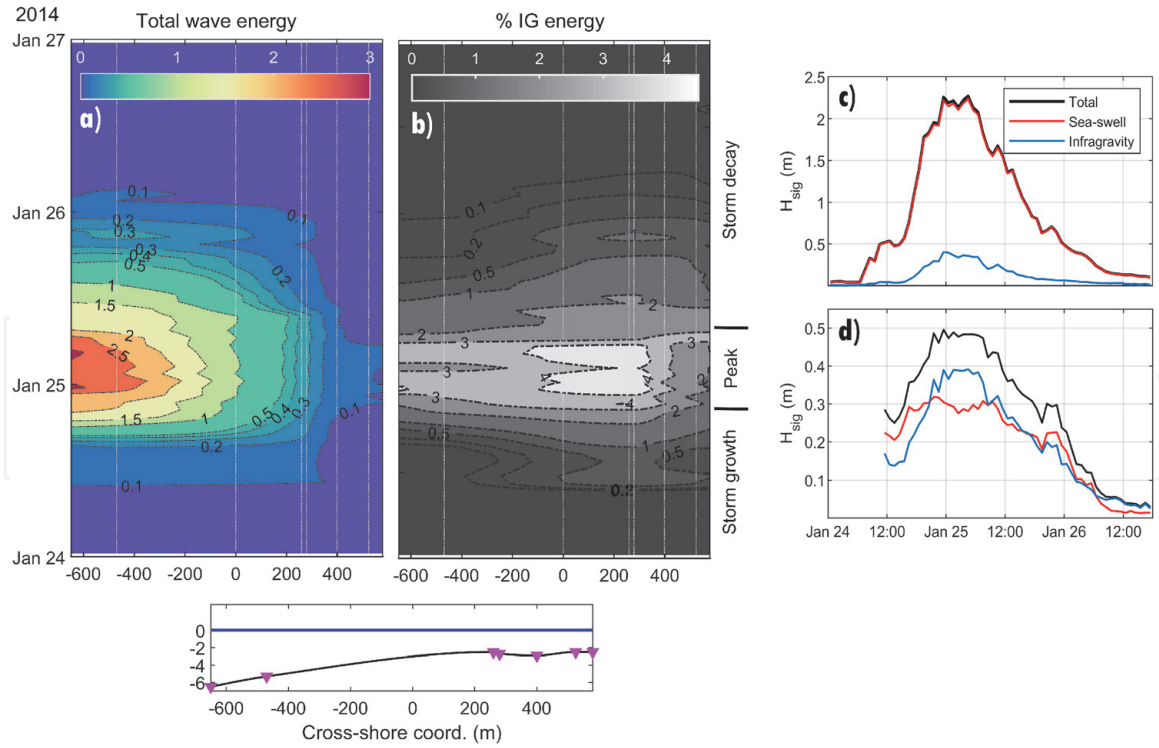


**Figure 4.**

Temporal and spatial evolution of wave energy during 24–26 January 2014: (a) total energy, (b) percentage of sea-swell contribution, (c) percentage of IG contribution. Evolution of band-specific significant wave height (d) in the offshore area, at QS2, and (e) in the river, at QR2. The bottom panel shows a schematic of the bed profile at the estuary and further offshore. Purple triangles represent the sensor location ( $x = 0$  m at the river mouth,  $x > 0$  moving upriver).

probably the bound wave mechanism [10], as suggested by a normalized slope parameter calculated off the mouth

$$\beta_b = \frac{h_x}{\omega} \sqrt{\frac{g}{h}} = 0.010 - 0.014 \quad (1)$$

where  $\omega = 0.63$  Hz is the wave angular frequency during the storm climax,  $g$  is the gravity acceleration,  $h_x = 1/200$  is the mean seabed slope, while  $h = (3 - 6)$  m is the depth range off the MR mouth.

It was observed that, while the IG contribution in the open sea was significantly smaller than that provided by sea-swell waves, it gained a more relevant role within the final reach of the MR. This is exemplified in **Figure 4c** and **d**, which shows the time evolution of band-specific significant wave heights during the storm event occurred on 25–26 January 2014, at two locations representative of offshore (QS2) and riverine (QR2) areas. While the total wave height in the sea was mainly due to sea-swell throughout the storm (**Figure 4c**), the IG contribution was seen to be much more important in the MR, especially during the storm climax (**Figure 4d**). This is due to the intense wave breaking affecting the shortest wave components at the mouth, and further enhanced by strong opposing currents. Inspection of wave energy levels revealed a large energy decay across a wide region off the MR mouth (between  $-400$  m and  $0$  m, at  $(2-5)$  m depths, as shown in **Figure 4a**). This decay especially involved the short-wave components, while the normalized IG component seemed to peak just past the MR mouth and values larger than the reference offshore value characterize the region between  $0$  and  $200$  m upriver (**Figure 4b**). Such behavior is connected to the large damping and deviation of storm-driven sea currents promoted by the river discharge [51], not enough to block IG components.



Hence, the MR estuarine area removes higher-frequency waves and retains low-frequency energy, thus operating as a low-pass filter. This process has already been observed in field experiments carried out in other environments, like microtidal estuaries or energetic oceanic inlets [24, 25, 65].

Although IG waves were observed to propagate upriver for hundreds of meters and tide propagate upriver for kilometers, the interplay between such low-frequency modes is of importance, with the tide controlling the upriver propagation of IG components [65]. In addition, despite the low tidal range at the MR estuary (less than 0.6 m during the January 2014 experiment), tidal oscillations reach distances larger than 1.2 km within the MR (e.g., at RG1), although tidal currents are low and their effect on the river current is negligible. While low-flow river conditions imposes very small resistance to the tide upriver propagation, the tidal forcing was easily suppressed by river floods and high-flow conditions [26, 51]. Furthermore, the tidal effect is important just off the estuary, in connection to a persistence of wave-induced setup during the storm decay.

On the other hand, no tidal influence was observed at RG2, as confirmed by more recent observations performed in 2019 (Figure 5a–c) [52]. These observations also confirmed the presence of tide at RG1, as well as the upriver propagation of additional low-frequency modes. Specifically, the stream-gauge recordings of some flood events occurred in 2019 allowed for the observation of modes not detected by the hydrometer, due to the difference in the sampling rate of the two instruments (2' for the stream gauge versus 30' for the hydrometer). The spectral content of two storm events recorded by the stream gauge and lasting a bit more than one day each (12–13 and 15–16 November 2019) has been analyzed, in conjunction with the spectral content of the signals recorded by both hydrometers (RG1 and RG2) and the tide gauge (Figure 5d). A long-time range has been used for hydrometer and tide signals, i.e. between 10 September and 17 December 2019. The hydrometers at RG1 and RG2 showed a similar spectral pattern, especially for frequencies  $f > 0.5 \cdot 10^{-4}$  Hz, while significant differences occurred for  $f < 0.5 \cdot 10^{-4}$  Hz, due to diurnal ( $\sim 25.6$  h) and semi-diurnal ( $\sim 12.8$  h) tidal constituents observed at RG1, but not at RG2.

Furthermore, the analysis of the stream-gauge signals during the recorded events at RG1 does not show relevant peaks referring to tidal constituents, due to

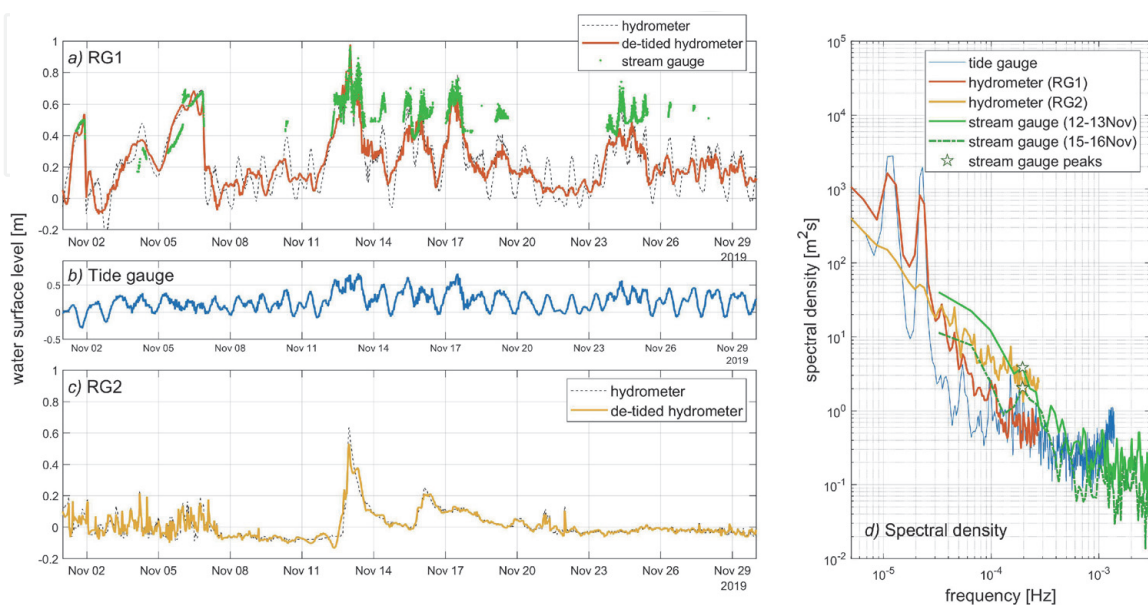


**Figure 5.** Time series recorded in 2019 by: (a) hydrometer and stream gauge at RG1, (b) tide gauge at Senigallia harbor, (c) hydrometer at RG2. (d) Spectral density of recorded signals.

the reduced event duration. However, local peaks exist at  $\sim 1.42$  hours during both events, which can be probably ascribed to other long-wave modes generating in the Adriatic Sea. Enclosed and semi-enclosed basins, like the Adriatic Sea, show low-frequency oscillations like the seiche motion, which can be described by the natural period at a specific mode  $n$ :

$$T_{seiche,n} = \frac{2L}{n\sqrt{gh}} \quad (2)$$

Selecting the mode-2 oscillation ( $n = 2$ ), with  $L \sim 130$  km being the transversal basin length and  $h = (50-70)$  m being a representative water depth along the transversal direction, Eq. (2) yields  $T_{seiche,n} = (1.38 - 1.63)$  hours. Hence, the peak period observed in **Figure 5d** falls in the calculated range and can be thus motivated by the transversal oscillation of the Adriatic basin, only detectable using high-frequency recordings during flood conditions. This might suggest that seiche modes are not particularly relevant in the long term, but they cannot be neglected during short-term events (order of hours to days).

### 3.4 River mouth bar

The dynamics of river mouth bars is strongly correlated with the mutual interaction of the river discharge and wave actions. The long-term monitoring of the MR estuary allowed us to correlate the behavior of the emerged mouth bar with the river and sea forcing. Hourly videos recorded by the SGS video-monitoring station were post-processed to create a 10-minute time-exposure image (timex). For each hour, the four timex images were stabilized, geo-rectified and merged to obtain the plan-view images. The ortho-rectified timex images, from 2017 to 2019, were analyzed using a semi-automatic procedure<sup>1</sup> to detect the presence of the emerged bar and its geometric features. The evolution of the area and center of mass of the bar was correlated with the sea state (wave height and direction) time-series recorded by the offshore ADCP, the tidal levels, as well as flow rate and water level recorded along the MR.

The results showed a net downriver migration due to relevant flood events (**Figure 6e-h**) and a persistence of sediment accumulation during periods of weak river action. Moreover, the accurate monitoring made it possible to observe a slow upriver bar migration under wave action (**Figure 6a-d**). Numerical modeling of the MR estuary, performed by Delft3D software, also highlighted the link between river discharge and downriver bar migration, and between wave action and upriver bar migration [54].

### 3.5 Coastal impact

The evolution of submerged sand bars may well be crucially altered (intentionally or not) by the presence of man-made structures, like breakwaters or jetties, the latter of which are commonly present in riverine environments [66, 67]. Melito et al. [4] discussed sandbar dynamics and their correlations with incident wave climate and morphological constraints at a portion of sheltered beach south of the MR estuary (**Figures 1b** and 7). The beach object of the study is delimited, at its northern side, by the southern concrete jetty delimiting the final reach of the MR. The jetty provides a partial sheltering from wave attack coming from northern

<sup>1</sup> <https://github.com/Coastal-Imaging-Research-Network/River-Bar-Toolbox>

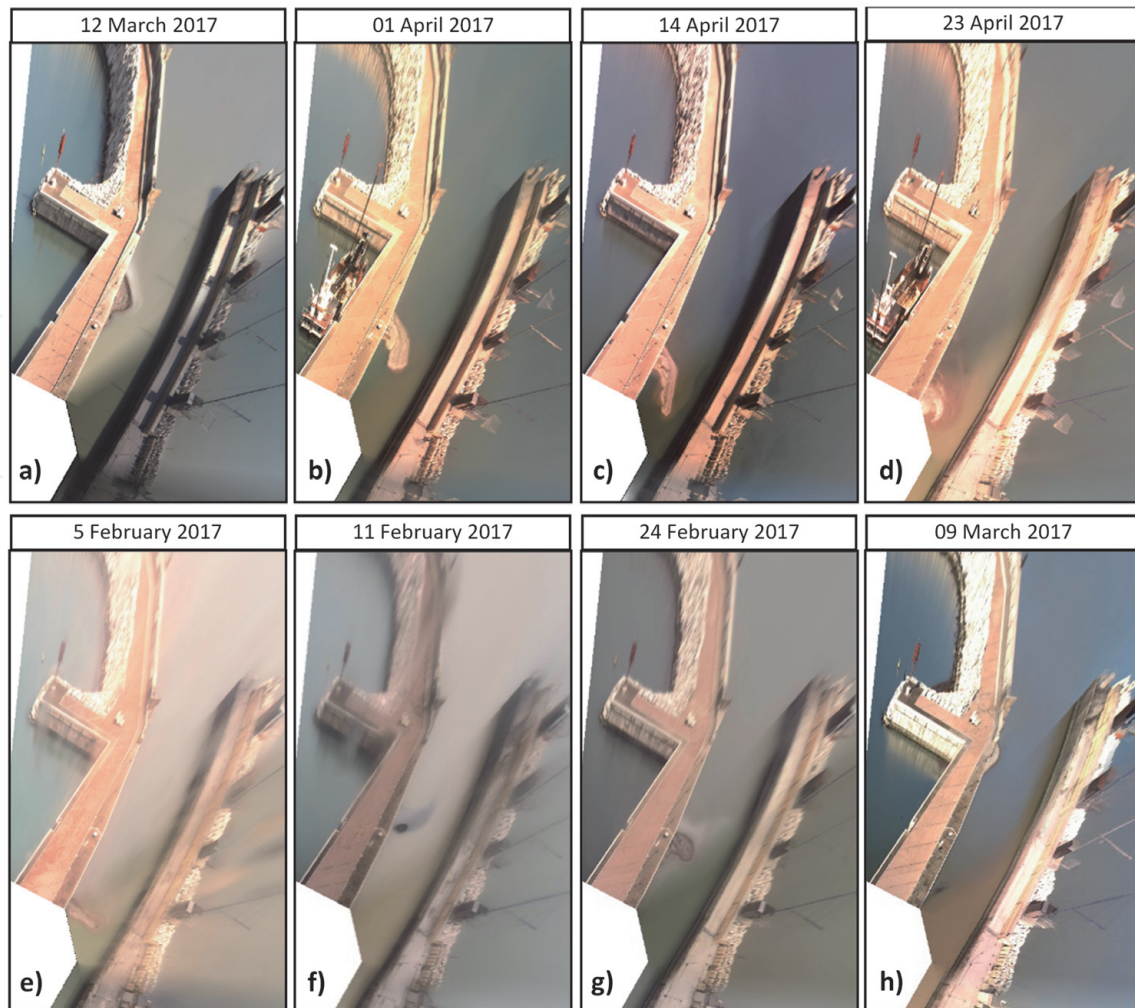


**Figure 6.** Ortho-rectified timex images recorded from the SGS video-monitoring station. (a, b, c, d) is an example of observed upriver migration. (e, f) and (g, h) are two examples of observed downriver migration.

quadrants (mainly originated by Bora storms), but leaves the coastline exposed to incident waves from eastern directions.

The submerged beach is characterized by an array of three shallow bars, whose displacement in response to seasonal climate and storm events is monitored since 2015 with the aid of remote sensing products from the SGS station. The bars at the sheltered beach show a response dominated by seasonal oscillations in wave climate, presenting occasionally consistent onshore displacements in milder climates typical of summer months, and offshore migration in winter months. The bar array is generally poorly responsive to single storms; a circumstance shared with other portions of unprotected coastline far from the influence of the river jetty. The overall behavior of the bar structure can be therefore assimilated to a pattern of bars oscillating around a more or less well-defined point of equilibrium (OPE pattern) [68].

Two short storm events from SSE occurred in February 2016 and October 2018, however, imposed a remarkable change in this established pattern by generating storm-scale displacements in the order of 30–50 m to all submerged bars. Migrations of such entity and with such short response times are not repeated anytime during the investigation period, spanning from 2015 to 2019, even during much more intense wave attacks. This exceptional event is likely connected to the peculiar interaction between incoming waves from eastern directions and the presence of the concrete jetty. Storm waves approach almost normally to the river jetty,



generating enhanced reflection and intensified return currents, ultimately leading to enhanced offshore displacements of bars.

The eventuality of different beach response to storm waves with different incidence was explored with a campaign of numerical simulations run with FUNWAVE [69] and focused on the interaction of the man-made landmark with the dominant wave field at the MR estuary [4]. Two simulations were devised to represent wave attacks from a typical Bora storm (NNE direction) and a typical Sirocco storm (ESE). The two prototypical storms used as wave input are rather different in terms of wave period: while the Bora storm is characterized by steeper waves ( $H_s = 2.28$  m,  $T_p = 7.6$  s) due to the more intense wind and limited fetch from northern quadrants, the Sirocco-driven storm features longer, swell-dominated waves ( $H_s = 2.26$  m,  $T_p = 9.3$  s) thanks to an increased fetch distance. The two hydrodynamic simulations are run over a bathymetry generated using a DTM featuring two well-defined bars.

30-minute-averaged velocity fields and relative wave heights in the nearshore area delimited by the MR jetty are presented in **Figure 7** for the Bora (NNE) storm and the Sirocco (ESE) storm. The FUNWAVE model predicts longshore currents on top of the bar in both cases; however, while the current is directed towards the jetty during the Bora storm (**Figure 7c**), Sirocco waves force a stronger current, directed away from the jetty, and escaping the nearshore giving birth to a marked circulation

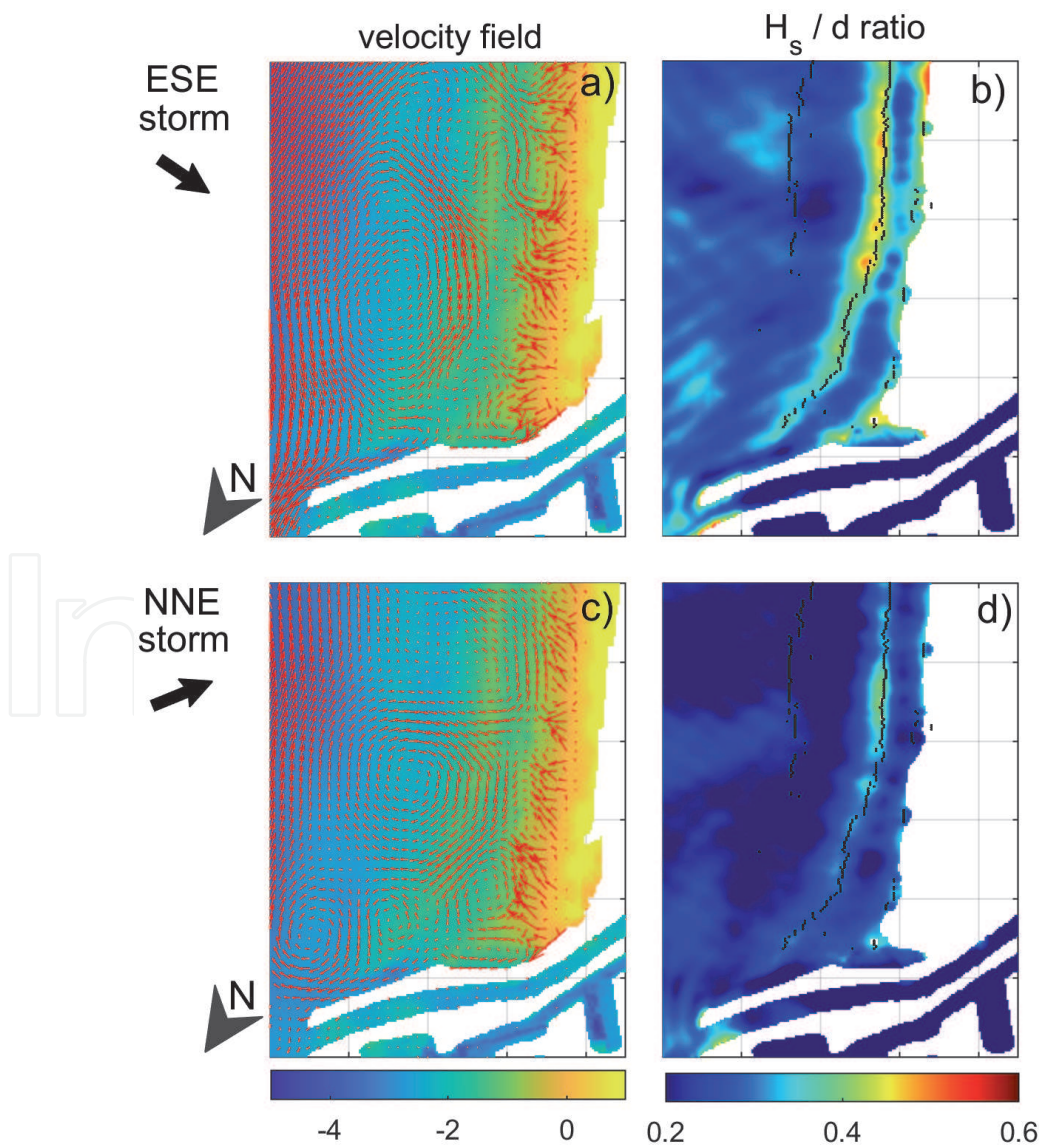


**Figure 7.** Numerical simulations of an ESE storm (a, b) and NNE storm (c, d). 30-minute-averaged velocity fields (a, c) and relative wave heights (b, d) in the nearshore area south of the MR jetty.

cell (**Figure 7a**). Stronger currents, along with higher relative wave heights over the bars for the Sirocco (ESE) event (**Figure 7b**) in comparison to those modeled during the Bora (NNE) event (**Figure 7d**), can thus be linked to a greater potential for sediment stirring and motion by Sirocco waves and, ultimately, bar migration during ESE storms.

#### 4. Discussion and concluding remarks

The overall dynamics of the salt-wedge estuary of the MR have been observed exploiting short-term measurements in both river and sea during September 2013 and January 2014, as well as long-term monitoring at different and farther locations. The short-term experiments revealed that the marine forcing is able at propagating upriver for long distances, during sea storms but also during relatively mild/quiescent conditions.

In detail, the large waves observed during both big and small storms propagated upriver for some hundreds of meters, also suggesting the existence of a TMZ developing at different locations within the MR, similar to what observed in meso- and macro-tidal estuaries [57, 59]. Further, results of the FM in the final reach of the MR suggest a fast macrofloc settling and high flocculation occurring about 600 m upriver of the mouth during the small storm, and an efficient flocculation throughout the range of turbulent stimulation, while both lower-river and seaward zones were characterized by a much smaller MSF compared to that estimated inland [57]. The impact of waves in the estuarine area is also suggested by the relevant seabed variations obtained comparing the bathymetric surveys of September 2013 and January 2014, which show significant erosion/deposition patterns just off the jetty (bed variations of  $\pm 1.5$  m), as well as important changes in the final river reach (erosion up to 1 m) [51].

However, the wave forcing is not the only action that pushes upriver marine waters along the MR. Evidence of the upriver propagation of marine fluxes was given in the summertime experiment (September 2013), when the salinity level in the MR, at about 1.8 km from the mouth, was larger than zero and suggested the existence of a flocculation zone at about (1.8–0.6) km from the mouth. Further, a floc deposition was supposed to occur in the final 600 m of the MR, as also demonstrated by the seabed increase and sediment deposition occurred in the 2013 summer, between May and September [50, 51]. In addition, more recent observations confirmed that the marine forcing can propagate upriver for kilometers, although not as IG waves, which mainly affect the final reach of the MR like the sea-swell waves do, as observed during the January 2014 storms [26]. Differently, very low-frequency waves like tides or seiches ( $T \sim 1.4$  hours) were recorded 1.2 km from the estuary and strongly affected the local hydrodynamics, being the water surface level generally more altered by tidal excursion than by river forcing during low-flow/quiescent conditions [52].

In terms of sediment transport and bed morphology, river mouth bars and coastal sandbars are directly linked to the forcing actions existing in the investigated microtidal area. The interplay among such actions is summarized by the evolution of a river mouth bar. While significant flood events promote a net downriver migration, a slow upriver bar migration is observed under wave action.

Linked to the main processes occurring within river and estuary are also the dynamics characterizing the coastal area just south of the MR jetty, where submerged sandbars evolve while protecting the natural beach. While the sediment supply from the MR significantly affects the sediment transport in such area, the main incoming direction of sea storms is thought to largely affect the SSC just off

the estuary. Numerical hydrodynamic simulations suggested that during NNE storms a recirculation cell is generated south of the jetty and over the sandbars, while the velocity field at the estuary is relatively small [4]. Hence, the river-induced plume propagating far offshore from the estuary seems to be not significantly affected by NNE waves, whereas a different velocity field seems to generate during ESE storms, providing a seaward-directed fast flow in correspondence of the jetty. Hence, on the one side, the MR plume seems to be enhanced by the wave-induced cross-shore current. On the other side, the sandbar array is supposed to evolve and migrate, due to a larger relative height over the bars themselves and possibly related sediment mobilization.

Many of the above-described aspects, especially the main processes related to the evolution of river mouth bars and river plume, as well as the accurate spatial analysis of the sea-forcing propagation within the MR during mild and stormy conditions, are currently under investigation and will be detailed in future contributions.

## **Acknowledgements**

The financial support from the MORSE Project (Office of Naval Research Global - UK, Research Grant Number N62909-17-1-2148) and the FUNBREAK Project (MIUR PRIN 2017 - Italy, Grant Number 20172B7MY9) is gratefully acknowledged. AJM's contribution towards this research was partly supported by the US National Science Foundation under grants OCE-1736668 and OCE-1924532, and HR Wallingford company research FineScale project (ACK3013\_62). The authors would like to thank all colleagues who made significant contributions during the planning and execution of the field experiments, as well as for the following activities, including Edward F. Braithwaite III, Sara Corvaro, Giovanna Darvini, Michael Fuller, Kevin Lois, Carlo Lorenzoni, Alessandro Mancinelli, Pierluigi Penna, Allen Reed, Aniello Russo, Alex Sheremet, Luciano Soldini, Tracy Staples, Gianluca Zitti. The following authorities and companies are also acknowledged: the Municipality of Senigallia, the Capitaneria di Porto of Senigallia and of Ancona, MARIDIPART La Spezia and MARIFARI Venezia, GESTIPOINT (Senigallia), Club Nautico (Senigallia), NOTA srl (Senigallia), Carmar Sub (Ancona), Sena Gallica (Senigallia), METIS S.R.L. (Senigallia). The data used in this paper are available at this link.

## **Conflict of interest**

The authors declare no conflict of interest.



IntechOpen

## Author details

Maurizio Brocchini<sup>1,2</sup>, Matteo Postacchini<sup>1\*</sup>, Lorenzo Melito<sup>1</sup>, Eleonora Perugini<sup>1</sup>, Andrew J. Manning<sup>2,3,4,5,6,9</sup>, Joseph P. Smith<sup>7</sup> and Joseph Calantoni<sup>8</sup>

1 Università Politecnica delle Marche, Ancona, Italy

2 University of Florida, Gainesville, FL, USA

3 HR Wallingford, Coasts and Oceans Group, Wallingford, UK

4 Environment and Energy Institute, University of Hull, Hull, UK

5 Stanford University, Stanford, California, USA

6 University of Delaware, Delaware, USA

7 Oceanography Department, U.S. Naval Academy, Annapolis, MD, USA


8 Ocean Sciences Division, U.S. Naval Research Laboratory, Stennis Space Center, MS, USA

9 University of Plymouth, Plymouth, UK

\*Address all correspondence to: [m.postacchini@staff.univpm.it](mailto:m.postacchini@staff.univpm.it)

## IntechOpen

---

© 2021 The Author(s). Licensee IntechOpen. This chapter is distributed under the terms of the Creative Commons Attribution License (<http://creativecommons.org/licenses/by/3.0/>), which permits unrestricted use, distribution, and reproduction in any medium, provided the original work is properly cited. 

## References

- [1] G. Dodet, X. Bertin, N. Bruneau, A.B. Fortunato, A. Nahon, A. Roland, Wave-current interactions in a wave-dominated tidal inlet, *J. Geophys. Res. Ocean.* (2013). <https://doi.org/10.1002/jgrc.20146>.
- [2] M. Olabarrieta, W.R. Geyer, N. Kumar, The role of morphology and wave-current interaction at tidal inlets: An idealized modeling analysis, *J. Geophys. Res. Ocean.* (2014). <https://doi.org/10.1002/2014JC010191>.
- [3] L. Melito, M. Postacchini, A. Sheremet, J. Calantoni, G. Zitti, G. Darvini, M. Brocchini, Wave-Current Interactions and Infragravity Wave Propagation at a Microtidal Inlet, *Proceedings.* (2018). <https://doi.org/10.3390/proceedings2110628>.
- [4] L. Melito, L. Parlagreco, E. Perugini, M. Postacchini, S. Devoti, L. Soldini, G. Zitti, L. Liberti, M. Brocchini, Sandbar dynamics in microtidal environments: Migration patterns in unprotected and bounded beaches, *Coast. Eng.* (2020). <https://doi.org/10.1016/j.coastaleng.2020.103768>.
- [5] M. Brocchini, Wave-forced dynamics in the nearshore river mouths, and swash zones, *Earth Surf. Process. Landforms.* (2020). <https://doi.org/10.1002/esp.4699>.
- [6] W.H. Munk, Origin and Generation of Waves, *Coast. Eng. Proc.* 1 (1950) 1. <https://doi.org/10.9753/icce.v1.1>.
- [7] R. Davidson-Arnott, *An Introduction to Coastal Processes and Geomorphology*, 2009. <https://doi.org/10.1017/cbo9780511841507>.
- [8] M. Tucker, Surf beats: sea waves of 1 to 5 min. period, *Proc. R. Soc. London. Ser. A. Math. Phys. Sci.* 202 (1950) 565–573. <https://doi.org/10.1098/rspa.1950.0120>.
- [9] G. Symonds, D.A. Huntley, A.J. Bowen, Two-dimensional surf beat: long wave generation by a time-varying breakpoint., *J. Geophys. Res.* (1982). <https://doi.org/10.1029/JC087iC01p00492>.
- [10] X. Bertin, A. de Bakker, A. van Dongeren, G. Coco, G. André, F. Ardhuin, P. Bonneton, F. Bouchette, B. Castelle, W.C. Crawford, M. Davidson, M. Deen, G. Dodet, T. Guérin, K. Inch, F. Leckler, R. McCall, H. Muller, M. Olabarrieta, D. Roelvink, G. Ruessink, D. Sous, É. Stutzmann, M. Tissier, Infragravity waves: From driving mechanisms to impacts, *Earth-Science Rev.* (2018). <https://doi.org/10.1016/j.earscirev.2018.01.002>.
- [11] K.M. Wijnberg, A. Kroon, Barred beaches, *Geomorphology.* (2002). [https://doi.org/10.1016/S0169-555X\(02\)00177-0](https://doi.org/10.1016/S0169-555X(02)00177-0).
- [12] B.G. Ruessink, J.H.J. Terwindt, The behaviour of nearshore bars on the time scale of years: A conceptual model, *Mar. Geol.* (2000). [https://doi.org/10.1016/S0025-3227\(99\)00094-8](https://doi.org/10.1016/S0025-3227(99)00094-8).
- [13] T.E. Baldock, P. Manoonvoravong, K.S. Pham, Sediment transport and beach morphodynamics induced by free long waves, bound long waves and wave groups, *Coast. Eng.* (2010). <https://doi.org/10.1016/j.coastaleng.2010.05.006>.
- [14] T. Aagaard, B. Greenwood, Suspended sediment transport and the role of infragravity waves in a barred surf zone, *Mar. Geol.* (1994). [https://doi.org/10.1016/0025-3227\(94\)90111-2](https://doi.org/10.1016/0025-3227(94)90111-2).
- [15] J.A. Roelvink, M.F.J. Stive, Bar-generating cross-shore flow mechanisms on a beach, *J. Geophys. Res.* (1989). <https://doi.org/10.1029/JC094iC04p04785>.
- [16] M. Postacchini, L. Soldini, C. Lorenzoni, A. Mancinelli, Medium-

Term dynamics of a middle Adriatic barred beach, *Ocean Sci.* 13 (2017). <https://doi.org/10.5194/os-13-719-2017>.

[17] L. Parlagreco, L. Melito, S. Devoti, E. Perugini, L. Soldini, G. Zitti, M. Brocchini, Monitoring for coastal resilience: Preliminary data from five Italian sandy beaches, *Sensors* (Switzerland). (2019). <https://doi.org/10.3390/s19081854>.

[18] T.C. Lippmann, R.A. Holman, Quantification of sand bar morphology: a video technique based on wave dissipation, *J. Geophys. Res.* (1989). <https://doi.org/10.1029/JC094iC01p00995>.

[19] M.S. Phillips, M.D. Harley, I.L. Turner, K.D. Splinter, R.J. Cox, Shoreline recovery on wave-dominated sandy coastlines: the role of sandbar morphodynamics and nearshore wave parameters, *Mar. Geol.* (2017). <https://doi.org/10.1016/j.margeo.2017.01.005>.

[20] T. Aagaard, J. Nielsen, B. Greenwood, Suspended sediment transport and nearshore bar formation on a shallow intermediate-state beach, *Mar. Geol.* (1998). [https://doi.org/10.1016/S0025-3227\(98\)00012-7](https://doi.org/10.1016/S0025-3227(98)00012-7).

[21] T. Sunamura, I. Takeda, Landward Migration of Inner Bars, *Dev. Sedimentol.* (1984). [https://doi.org/10.1016/S0070-4571\(08\)70141-9](https://doi.org/10.1016/S0070-4571(08)70141-9).

[22] F. Hoefel, S. Elgar, Wave-induced sediment transport and sandbar migration, *Science* (80-. ). (2003). <https://doi.org/10.1126/science.1081448>.

[23] E.L. Gallagher, S. Elgar, R.T. Guza, Observations of sand bar evolution on a natural beach, *J. Geophys. Res. Ocean.* (1998). <https://doi.org/10.1029/97jc02765>.

[24] R.J. Uncles, J.A. Stephens, C. Harris, Infragravity currents in a small ria:

Estuary-amplified coastal edge waves?, *Estuar. Coast. Shelf Sci.* (2014). <https://doi.org/10.1016/j.ecss.2014.04.019>.

[25] M.E. Williams, M.T. Stacey, Tidally discontinuous ocean forcing in bar-built estuaries: The interaction of tides, infragravity motions, and frictional control, *J. Geophys. Res. Ocean.* (2016). <https://doi.org/10.1002/2015JC011166>.

[26] L. Melito, M. Postacchini, A. Sheremet, J. Calantoni, G. Zitti, G. Darvini, P. Penna, M. Brocchini, Hydrodynamics at a microtidal inlet: Analysis of propagation of the main wave components, *Estuar. Coast. Shelf Sci.* 235 (2020). <https://doi.org/10.1016/j.ecss.2020.106603>.

[27] V.N. Mikhailov, Hydrology and formation of river-mouth bars, in: *Probl. Humid Trop. Zo. Deltas*, 1966: pp. 59–64. <ftp://ftp.ems.psu.edu/data/pub/geosc/pub/dedmonds/Mikhailov197.pdf>.

[28] L.D. Wright, Morphodynamics of a Wave-Dominated River Mouth, in: *Coast. Eng.* 1976, American Society of Civil Engineers, New York, NY, 1976: pp. 1721–1737. <https://doi.org/https://doi.org/10.9753/icce.v15.99>.

[29] S. Fagherazzi, D.A. Edmonds, W. Nardin, N. Leonardi, A. Canestrelli, F. Falcini, D.J. Jerolmack, G. Mariotti, J.C. Rowland, R.L. Slingerland, Dynamics of river mouth deposits, *Rev. Geophys.* (2015). <https://doi.org/10.1002/2014RG000451>.

[30] D.A. Edmonds, R.L. Slingerland, Mechanics of river mouth bar formation: Implications for the morphodynamics of delta distributary networks, *J. Geophys. Res. Earth Surf.* (2007). <https://doi.org/10.1029/2006JF000574>.

[31] H. Mitchener, H. Torfs, Erosion of mud/sand mixtures, *Coast. Eng.* (1996). [https://doi.org/10.1016/S0378-3839\(96\)00002-6](https://doi.org/10.1016/S0378-3839(96)00002-6).



- [32] T.S. Mostafa, J. Imran, M.H. Chaudhry, I.B. Kahn, Erosion resistance of cohesive soils, *J. Hydraul. Res.* (2008). <https://doi.org/10.3826/jhr.2008.2794>.
- [33] J.C. Winterwerp, W.G.M. van Kesteren, *Introduction to the Physics of Cohesive Sediment Dynamics in the Marine Environment*, 2004.
- [34] A.J. Mehta, *An introduction to hydraulics of fine sediment transport*, World Scientific Publishing Company, 2013.
- [35] A.J. Manning, J. V. Baugh, J.R. Spearman, R.J.S. Whitehouse, *Flocculation settling Characteristics of mud: Sand mixtures*, in: *Ocean Dyn.*, 2010. <https://doi.org/10.1007/s10236-009-0251-0>.
- [36] Manning, A.J., J.R. Spearman, R.J.S. Whitehouse, E.L. Pidduck, J.V. Baugh, K.L. Spencer, *Laboratory Assessments of the Flocculation Dynamics of Mixed Mud: Sand Suspensions*, in: A.J. Manning (Ed.), *Sediment Transp. Process. Their Model. Appl.*, InTech (Rijeka, Croatia), 2013: pp. 119–164. <https://doi.org/org/10.5772/3401>.
- [37] R. Whitehouse, R. Soulsby, W. Roberts, H. Mitchener, *Dynamics of estuarine muds*, 2000. <https://doi.org/10.1680/doem.28647>.
- [38] K.R. Dyer, *Coastal and estuarine sediment dynamics.*, (1986). [https://doi.org/10.1016/0378-3839\(88\)90018-x](https://doi.org/10.1016/0378-3839(88)90018-x).
- [39] A.J. Raudkivi, *Loose boundary hydraulics*, 1998. <https://doi.org/10.1139/l91-110>.
- [40] M. Van Ledden, *Sand-mud segregation in estuaries and tidal basins*, *Commun. Hydraul. Geotech. Eng.* (2003).
- [41] D.M. Paterson, S.E. Hagerthey, *Microphytobenthos in contrasting coastal ecosystems: Biology and dynamics*, in: K. Reise (Ed.), *Ecol. Comp. Sediment. Shores*, Berlin: Springer, 2001: pp. 105–125.
- [42] N. Tambo, Y. Watanabe, *Physical characteristics of flocs-I. The floc density function and aluminium floc*, *Water Res.* (1979). [https://doi.org/10.1016/0043-1354\(79\)90033-2](https://doi.org/10.1016/0043-1354(79)90033-2).
- [43] R.C. Klimpel, R. Hogg, *Effects of flocculation conditions on agglomerate structure*, *J. Colloid Interface Sci.* (1986). [https://doi.org/10.1016/0021-9797\(86\)90212-2](https://doi.org/10.1016/0021-9797(86)90212-2).
- [44] I.G. Droppo, D.E. Walling, E.D. Ongley, *The influence of floc size, density and porosity on sediment and contaminant transport*, in: *IAHS-AISH Publ.*, 2000.
- [45] G.G. Stokes, *On the effect of the Internal friction of fluids on the motion of pendulums - Section III*, *Trans. Cambridge Philos. Soc.* (1850).
- [46] K.R. Dyer, A.J. Manning, *Observation of the size, settling velocity and effective density of flocs, and their fractal dimensions*, in: *J. Sea Res.*, 1999. [https://doi.org/10.1016/S1385-1101\(98\)00036-7](https://doi.org/10.1016/S1385-1101(98)00036-7).
- [47] A.J. Manning, K.R. Dyer, *Mass settling flux of fine sediments in Northern European estuaries: Measurements and predictions*, *Mar. Geol.* (2007). <https://doi.org/10.1016/j.margeo.2007.07.005>.
- [48] R.L. Soulsby, A.J. Manning, J. Spearman, R.J.S. Whitehouse, *Settling velocity and mass settling flux of flocculated estuarine sediments*, *Mar. Geol.* (2013). <https://doi.org/10.1016/j.margeo.2013.04.006>.
- [49] A.J. Mehta, J.W. Lott, *Sorting of fine sediment during deposition*, in:

Coast. Sediments, ASCE, 1987:  
pp. 348–362.

[50] M. Brocchini, J. Calantoni, A.H. Reed, M. Postacchini, C. Lorenzoni, A. Russo, A. Mancinelli, S. Corvaro, G. Moriconi, L. Soldini, Summertime conditions of a muddy estuarine environment: The EsCoSed project contribution, *Water Sci. Technol.* 71 (2015). <https://doi.org/10.2166/wst.2015.116>.

[51] M. Brocchini, M. Postacchini, C. Lorenzoni, A. Russo, S. Corvaro, A. Mancinelli, L. Soldini, J. Calantoni, A.H. Reed, E.F. Braithwaite, A. Sheremet, T. Staples, J. Smith, Comparison between the wintertime and summertime dynamics of the Misa River estuary, *Mar. Geol.* 385 (2017). <https://doi.org/10.1016/j.margeo.2016.12.005>.

[52] M. Postacchini, L. Melito, A. Sheremet, J. Calantoni, G. Darvini, S. Corvaro, F. Memmola, P. Penna, M. Brocchini, Upstream Propagating Long-Wave Modes at a Microtidal River Mouth, *Environ. Sci. Proc.* (2020). <https://doi.org/10.3390/environsciproc2020002015>.

[53] A. Valle-Levinson, Contemporary issues in estuarine physics, 2010. <https://doi.org/10.1017/CBO9780511676567>.

[54] A. Baldoni, E. Perugini, L. Soldini, J. Calantoni, M. Brocchini, Long-term evolution of an inner bar at the mouth of a microtidal river, *Estuar. Coast. Shelf Sci.* (under review).

[55] Deltares, Delft3D-FLOW. Simulation of multi-dimensional hydrodynamic flows and transport phenomena, including sediments. User Manual. Hydro-Morphodynamics. Version: 3.15.34158, 2014.

[56] Deltares, Delft3D-Wave, Simulation of short-crested waves with SWAN,

User Manual, Version 3.05.58426, Deltares. (2019) 200.

[57] M. Postacchini, A.J. Manning, J. Calantoni, J.P. Smith, M. Brocchini, A Storm Driven Turbidity Maximum in a Microtidal Estuary, *J. Geophys. Res. Ocean.* (under review).

[58] R.J. Uncles, R.C.A. Elliott, S.A. Weston, Observed fluxes of water, salt and suspended sediment in a partly mixed estuary, *Estuar. Coast. Shelf Sci.* (1985). [https://doi.org/10.1016/0272-7714\(85\)90035-6](https://doi.org/10.1016/0272-7714(85)90035-6).

[59] R.J. Uncles, J.A. Stephens, Nature of the turbidity maximum in the Tamar Estuary, U.K., *Estuar. Coast. Shelf Sci.* (1993). <https://doi.org/10.1006/ecss.1993.1025>.

[60] A.J. Manning, W.J. Langston, P.J.C. Jonas, A review of sediment dynamics in the Severn Estuary: Influence of flocculation, *Mar. Pollut. Bull.* (2010). <https://doi.org/10.1016/j.marpolbul.2009.12.012>.

[61] J. Spearman, A.J. Manning, On the significance of mud transport algorithms for the modelling of intertidal flats, in: *Proc. Mar. Sci.*, 2008. [https://doi.org/10.1016/S1568-2692\(08\)80030-7](https://doi.org/10.1016/S1568-2692(08)80030-7).

[62] A.J. Manning, J. V. Baugh, J.R. Spearman, E.L. Pidduck, R.J.S. Whitehouse, The settling dynamics of flocculating mud-sand mixtures: Part 1- Empirical algorithm development, in: *Ocean Dyn.*, 2011. <https://doi.org/10.1007/s10236-011-0394-7>.

[63] R.B. Krone, A study of rheologic properties of estuarial sediments, 1963.

[64] D. Eisma, Flocculation and deflocculation of suspended matter in estuaries, *Netherlands J. Sea Res.* (1986). [https://doi.org/10.1016/0077-7579\(86\)90041-4](https://doi.org/10.1016/0077-7579(86)90041-4).

[65] X. Bertin, M. Olabarrieta, Relevance of infragravity waves in a wave-dominated inlet, *J. Geophys. Res. Ocean.* (2016). <https://doi.org/10.1002/2015JC011444>.

[66] M. Sedrati, P. Ciavola, J. Reyns, C. Armaroli, V. Sipka, Morphodynamics of a microtidal protected beach during low wave-energy conditions, in: *J. Coast. Res.*, 2009.

[67] C. Bouvier, B. Castelle, Y. Balouin, Modeling the impact of the implementation of a submerged structure on surf zone sandbar dynamics, *J. Mar. Sci. Eng.* (2019). <https://doi.org/10.3390/jmse7040117>.

[68] R. Certain, J.P. Barusseau, Conceptual modelling of sand bars morphodynamics for a microtidal beach (Sète, France), *Bull. La Soc. Geol. Fr.* (2005). <https://doi.org/10.2113/176.4.343>.

[69] F. Shi, J.T. Kirby, J.C. Harris, J.D. Geiman, S.T. Grilli, A high-order adaptive time-stepping TVD solver for Boussinesq modeling of breaking waves and coastal inundation, *Ocean Model.* (2012). <https://doi.org/10.1016/j.ocemod.2011.12.004>.